Kinematics of Parsec-Scale Jets of Three Gamma-Ray Blazars at 43 GHz: 2013-2018 Behavior

Weaver, Z.R.[1], Jorstad, S.G.[1,2], Marscher, A.P.[1]

1. Boston University, USA; 2. St. Petersburg State University, Russian Federation

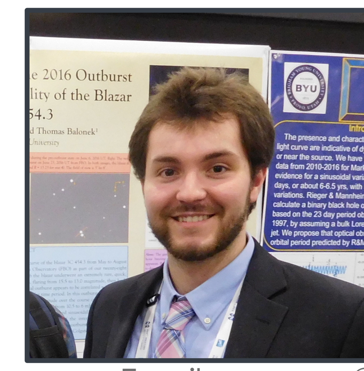

Website

ORCID

Email: zweaver@bu.edu

Abstract

We analyze the parsec-scale jet kinematics from 2013 January to 2017 December of the gamma-ray bright blazars 4C +21.35 (PKS 1222+216), 3C 279, and PKS 1510-089, monitored roughly monthly with the Very Long Baseline Array (VLBA) at 43 GHz. In a total of 158 images, we measure apparent speeds of 19 emission knots, of which 4 are quasi-stationary. Using the apparent speeds of the components and the timescales of variability from their light curves, we derive the physical parameters of the 15 superluminal knots, including variability Doppler factors, Lorentz factors, and viewing angles. We estimate the half-opening angle of each jet based on the projected opening angle and viewing angle. We calculate the intrinsic brightness temperatures of the cores at all epochs. We finally discuss the changes in jet behavior of these jets compared to their behavior during the time period 2007 June to 2013 January, as described in Jorstad et al. (2017).

Acknowledgements

This research is supported in part by NASA Fermi Guest Investigator grant 80NSSC17K0649 and by the NRAO student support program.

Jet Structure & Knot Identification

Details of the observations made with the VLBA can be found in Jorstad et al. (2017). We follow the traditional approach to model the total intensity visibility files (e.g., Homan et al. 2001, Jorstad et al. 2001, Jorstad et al. 2017). We represent the total structure of each source at each epoch with a series of 2D Gaussian components that best fit the visibility data determined by iterations with the MODELFIT task in Difmap. The component parameters are flux density, S, distance with respect to the core, R, relative position angle (measured north through east), Θ_{obs}, and angular size, a. The brightness temperature, $T_{b,obs}$, is then derived through the method described in Jorstad et al. 2005. Features are then correlated across epochs by searching for continuity in the fitted parameters. Polynomials of degree $\ell = 0, 1, \text{or } 2$ are then fit to the X and Y coordinate of each knot, and the best fit is determined by a χ^2 test. Average parameters for the structure features of the knots for each source are found in Table 1 (left), and seen in Fig. 1-3 for 1222+216, Fig. 4-6 for 3C 279, and Fig. 7-9 for 1510-089.

Table 1: Jet Structure

Source	Knot	N	$\langle S\rangle$ Jy	$\langle R\rangle$ mas	$\langle\Theta\rangle$ deg	$\langle a\rangle$ mas	Type
1222+216	A0	49	0.63 ± 0.39	0.0	0.0	0.10 ± 0.08	Core
	A1	46	0.32 ± 0.17	0.18 ± 0.05	18.1 ± 18.1	0.05 ± 0.02	St
	A2	45	0.15 ± 0.08	0.45 ± 0.07	11.75 ± 15.1	0.18 ± 0.13	St
	B4	19	0.16 ± 0.06	1.59 ± 0.40	-2.33 ± 0.97	0.33 ± 0.06	M
	B5	24	0.21 ± 0.08	1.10 ± 0.24	15.07 ± 4.63	0.39 ± 0.17	M
	B6	42	0.20 ± 0.10	2.17 ± 0.78	-1.03 ± 1.10	1.04 ± 0.44	M
	B7	13	0.10 ± 0.04	1.72 ± 0.33	4.96 ± 2.35	0.45 ± 0.12	M
	B8	10	0.06 ± 0.02	0.94 ± 0.20	21.20 ± 1.50	0.17 ± 0.04	M
3C 279	A0	53	7.76 ± 1.64	0.0	0.0	0.13 ± 0.04	Core
	C33	42	1.84 ± 1.09	0.04 ± 0.08	-158.35 ± 4.72	0.28 ± 0.16	M
	C34	53	3.11 ± 2.76	0.86 ± 0.15	-152.28 ± 3.00	0.23 ± 0.07	M
	C35	18	0.45 ± 0.22	1.28 ± 0.31	-128.37 ± 3.35	0.53 ± 0.20	M
	C36	23	0.59 ± 0.41	1.64 ± 0.45	-146.26 ± 2.26	0.48 ± 0.23	M
	C37	17	0.23 ± 0.08	1.72 ± 0.14	-147.40 ± 1.72	0.27 ± 0.12	M
1510-089	A0	56	2.05 ± 0.80	0.0	0.0	0.10 ± 0.07	Core
	A3	18	0.35 ± 0.26	0.31 ± 0.09	-28.37 ± 11.35	0.20 ± 0.12	St
	A4	9	0.18 ± 0.09	0.76 ± 0.13	-22.32 ± 4.66	0.42 ± 0.24	St
	B6	6	0.11 ± 0.06	1.26 ± 0.18	-29.56 ± 3.80	0.42 ± 0.22	M
	B7	9	0.19 ± 0.04	0.85 ± 0.41	-33.72 ± 11.11	0.68 ± 0.33	M
	B8	19	0.99 ± 0.99	0.53 ± 0.18	-33.09 ± 6.52	0.32 ± 0.19	M
	B9	17	0.63 ± 0.58	1.42 ± 0.54	-38.70 ± 3.24	0.63 ± 0.29	M
	B10	5	0.12 ± 0.02	0.43 ± 0.10	-33.66 ± 5.11	0.23 ± 0.15	M

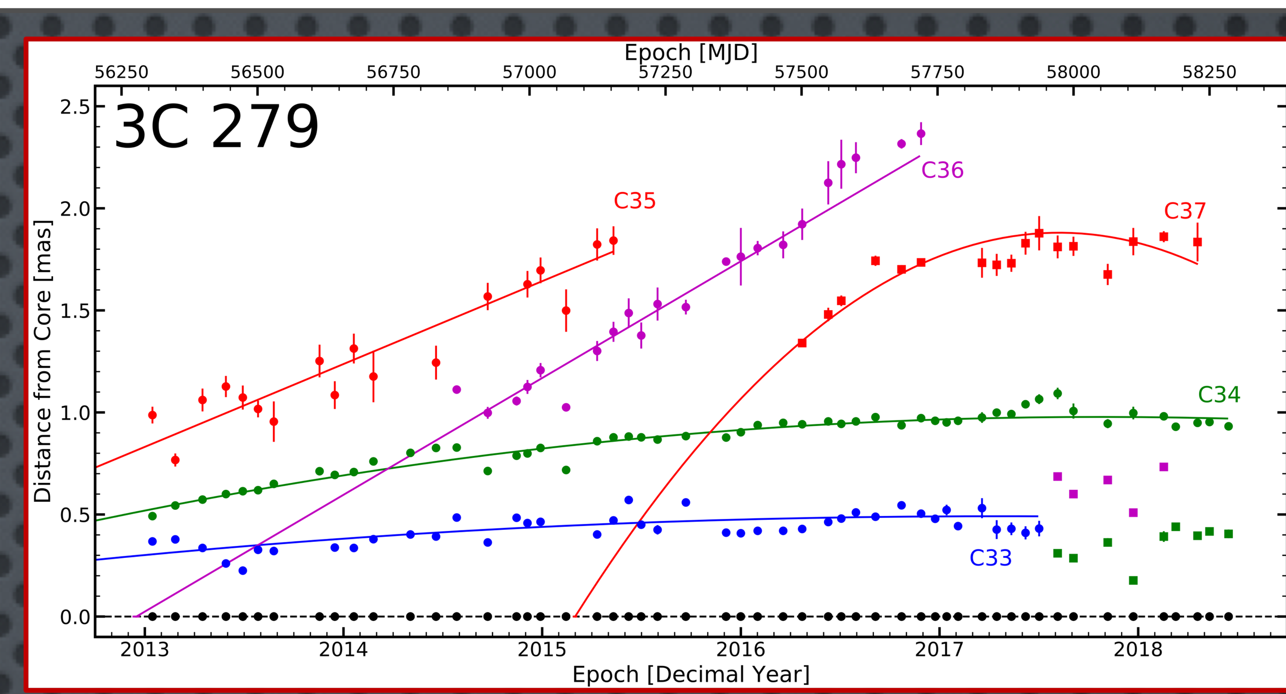

Fig. 4 (above). Separation of jet features from the core of 3C 279 from 2013 Jan. to mid-2018. The solid lines or curves represent polynomial fits to the motion, while the dotted line marks the position of the core. Error bars show the approximate 1σ positional uncertainties based on $T_{b,obs}$.

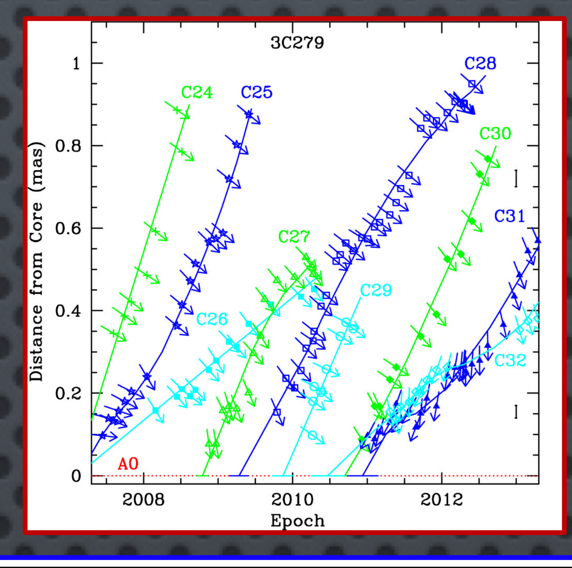

Fig. 5 (left). The separation of jet features from the core of 3C 279 from mid-2007 to mid-2012 (from Jorstad et al. 2017). The vectors show the P.A. of each knot with respect to the core at the corresponding epoch. The vertical black line segments show the approximate 1σ positional uncertainties based on $T_{b,obs}$.

Fig. 6 (right). Sample sequence of VLBA images of the quasar 3C 279. The size of the restoring beam is 0.15×0.36 mas² at a position angle of -10°. Contours decrease by a factor of $\sqrt{2}$ with respect to the peak flux density across all epochs, 8386 mJy beam⁻¹ on 2015 February 14. Straight lines across the images show the positions of the core *A0* and moving knots.

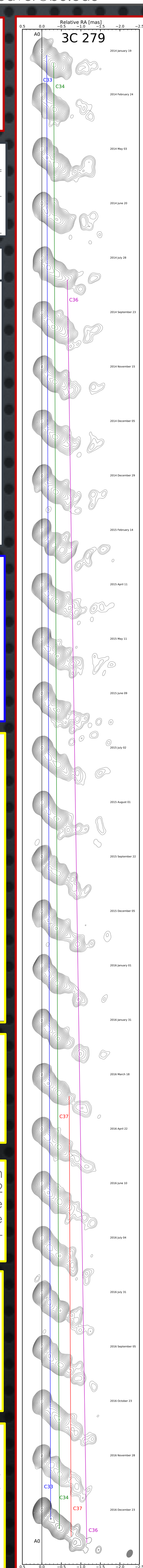

Table 5: 2007-2013 Physical Parameters of Jets (from Jorstad et al. 2017)

Source	D (Gpc)	$\langle\delta\rangle$	$\langle\Gamma\rangle$	$\langle\Theta_o\rangle$ (deg)	$T_{b,int}^{core}$ (10^{10} K)	θ_o (deg)	N
1222+216	2.379	7.4 ± 2.1	13.9 ± 2.1	5.6 ± 1.0	46.00	1.5 ± 1.0	3
3C279	3.080	18.3 ± 1.9	13.3 ± 0.6	1.9 ± 0.6	82.9	2.3 ± 2.2	3
1510-089	1.919	35.3 ± 4.6	22.5 ± 3.3	1.2 ± 0.3	14.1	0.5 ± 0.3	5

Past Behavior Comparison

The physical parameters of the jets for the time period mid-2007 to mid-2012 are given in Table 5 (above). The parsec-scale jets of 1222+216 and 1510-089 did not change dramatically between the two analyzed time periods, even though the quasi-stationary features do not line up between periods for 1510-089. The jet of 3C 279, however, appears to have shifted such that the angle between the jet axis and the line of sight is larger. This has correspondingly lowered the apparent speeds of knots moving down the jet.

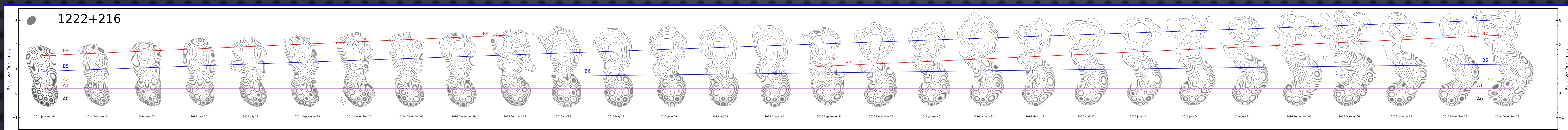

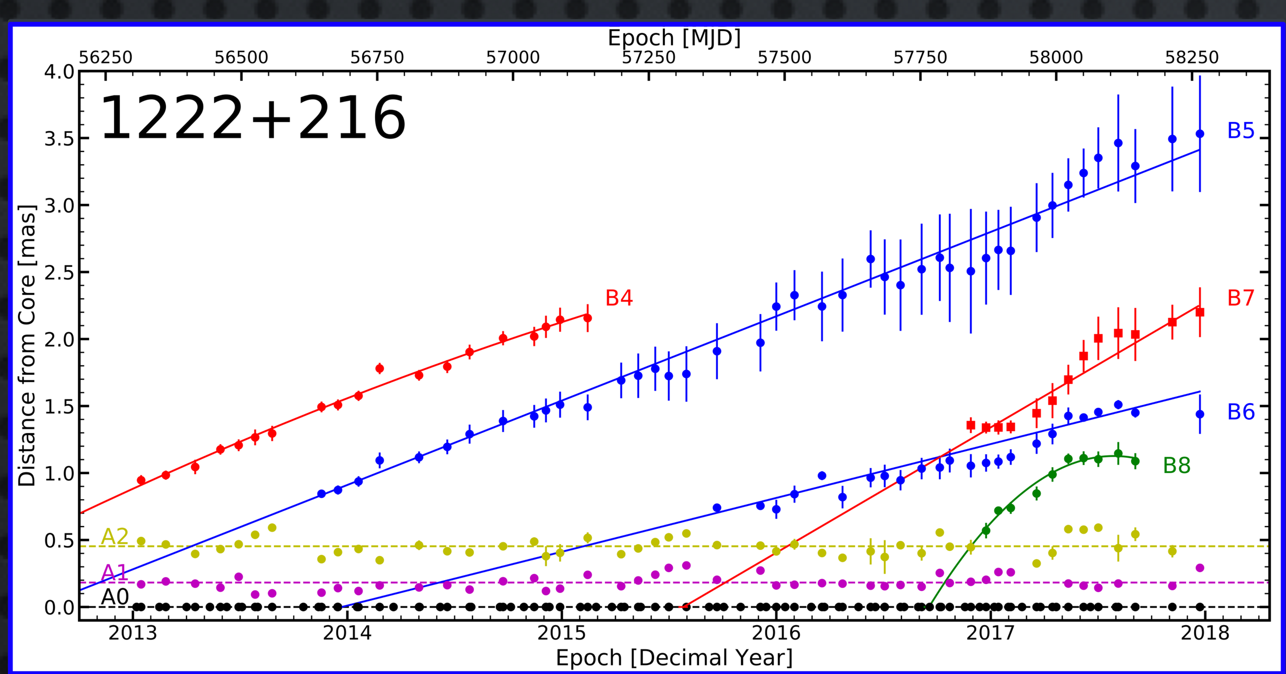

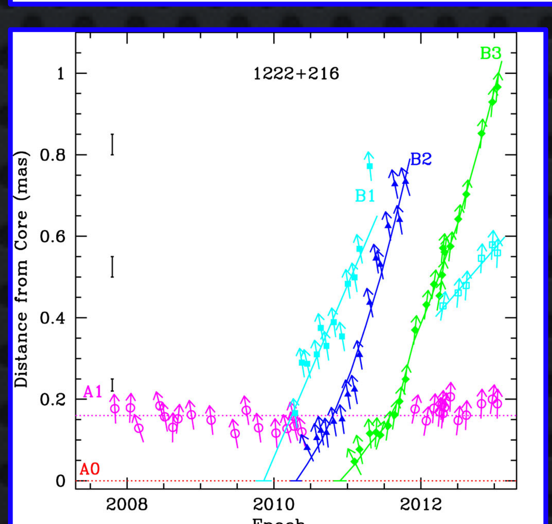

Fig. 2 (above). Separation of jet features from the core of 1222+216 from 2013 Jan. to 2017 Dec. The solid lines or curves represent polynomial fits to the motion, while the dotted line marks the position of the core and quasi-stationary features.. Error-bars show the approximate 1σ positional uncertainties based on $T_{b,obs}$.

Fig. 3 (left). The separation of jet features from the core of 1222+216 from mid-2007 to mid-2012 (from Jorstad et al. 2017). The vectors show the P.A. of each knot with respect to the core. The vertical black line segments show the approximate 1σ positional uncertainties based on $T_{b,obs}$.

Fig. 1 (above). Sample sequence of VLBA images of the quasar 1222+216. The size of the restoring beam is 0.16×0.36 mas² at a position angle of -10°. Contours decrease by a factor of $\sqrt{2}$ w.r.t. the peak flux density across all epochs, 1592 mJy beam⁻¹ on 2014 November 15. Straight lines across the images show the positions of the core *A0* & moving or quasi-stationary knots.

Knot Kinematics

The name of each knot is a continuation from Jorstad et al. (2017), where "A" knots are quasi-stationary features, "B" knots are moving features, and for 3C 279 the designations have continued from past analyses. Based on the polynomials that best fit the data, we calculate proper motion, μ, direction of motion, Φ, and apparent speed β_{app} for each knot, following the method in Jorstad et al. (2005). We then calculate the epoch of ejection T_0 for each knot with statistically significant proper motion. The degree of the fit in each coordinate, average proper motion, direction of motion, apparent speed, and epoch of ejection are provided in Table 2 (upper right).

Physical Parameters of Jets

Using the kinematics of each knot, we compute physical parameters in the parsec-scale jets of the sources. The average Doppler factor of variability, δ_{var}, is calculated using the formalism developed in Jorstad et al. (2005), using the angular size and timescale of variability, τ_{var}, of each knot and the luminosity distance and redshift of the source. To derive τ_{var}, we make use of the fact that the majority of AGN flares at millimeter wavelengths can be modeled by exponential profiles (Terasranta & Valtaoja 1994; Lister 2001). Thus, we fit a line to the ln(S) vs time graph of each knot, and take $\tau_{var} = |\frac{1}{k}|$ where k is the slope of the line. For knots with $\sigma_{\tau_{var}} < \tau_{var}/2$, we then calculate the Lorentz factor, Γ, and viewing angle, Θ_0, of each knot using the relations in Jorstad et al. (2017). Values for these parameters can be found in Table 3 (upper right). For each source, we then compute the total average Doppler factor, Lorentz factor, and viewing angle. These are shown in Table 4 (above), along with the maximum intrinsic brightness temperature of the core, $T_{b,int}^{core}$, intrinsic viewing angle $\theta_0 = (\max(\Theta_0) - \min(\Theta_0))/2$, and number of knots N.

Table 2: Velocities in Jets

Source	Knot	ℓ_x	ℓ_y	$\langle\mu\rangle$ mas yr^{-1}	$\langle\Phi\rangle$ deg	$\langle\beta_{app}\rangle$ c	T_0
1222+216	B4	1	1	0.631 ± 0.0004	-0.9 ± 0.002	16.75 ± 0.01	2011.88 ± 0.01
	B5	1	1	0.437 ± 0.0002	-36.5 ± 0.03	11.60 ± 0.01	2013.97 ± 0.01
	B6	2	1	0.658 ± 0.0002	-1.4 ± 0.002	17.47 ± 0.01	2012.55 ± 0.01
	B7	1	1	0.938 ± 0.009	-2.6 ± 0.2	24.90 ± 0.24	2015.57 ± 0.02
	B8	2	2	0.751 ± 0.004	-18.4 ± 0.2	19.94 ± 0.11	2016.71 ± 0.02
3C 279	C33	1	2	0.046 ± 0.0001	-135.2 ± 0.1	1.46 ± 0.003	2010.55 ± 0.01
	C34	2	2	0.085 ± 0.00001	-134.3 ± 0.01	2.71 ± 0.0003	2010.89 ± 0.1
	C35	1	1	0.406 ± 0.001	-149.3 ± 0.1	12.92 ± 0.03	2010.95 ± 0.01
	C36	1	1	0.570 ± 0.001	-129.6 ± 0.1	18.14 ± 0.03	2012.96 ± 0.01
	C37	2	2	0.206 ± 0.001	-145.5 ± 0.2	6.56 ± 0.03	2015.17 ± 0.01
1510-089	B6	1	1	0.953 ± 0.002	-32 ± 1.1	21.40 ± 0.04	2011.88 ± 0.01
	B7	1	1	1.674 ± 0.011	-23.3 ± 0.4	37.59 ± 0.25	2014.66 ± 0.06
	B8	2	2	0.159 ± 0.112	-1.3 ± 0.5	3.57 ± 2.52	2015.97 ± 0.11
	B9	2	2	1.070 ± 0.003	-27.1 ± 0.3	24.03 ± 0.07	2016.66 ± 0.06
	B10	1	1	1.116 ± 0.026	-34.9 ± 1	25.06 ± 0.58	2018.07 ± 0.02

Table 3: Physical Parameters of Jet Features

Source	Knot	τ_{var} years	δ_{var}	Γ	Θ_o deg
1222+216	B4	1.92 ± 0.02	6.87 ± 1.25	23.9 ± 0.9	5.9 ± 0.3
	B5	2.47 ± 0.14	6.31 ± 2.77	13.9 ± 0.3	7.6 ± 1.5
	B6	2.09 ± 0.01	19.88 ± 8.41	17.6 ± 4.7	2.9 ± 1.4
	B7	2.47 ± 0.14	7.28 ± 1.98	46.3 ± 4.4	4.2 ± 0.2
	B8	2.33 ± 1.30	2.91 ± 1.76	69.8 ± 19.4	5.6 ± 0.1
3C 279	C33	13.7 ± 0.70	1.04 ± 0.59	2.0 ± 0.01	52.9 ± 15.4
	C34	1.97 ± 0.01	5.92 ± 1.80	3.7 ± 1.2	7.5 ± 3.8
	C35	2.02 ± 0.07	13.30 ± 5.04	13.0 ± 2.6	4.3 ± 1.7
	C36	1.42 ± 0.02	17.14 ± 8.21	18.2 ± 3.9	3.3 ± 1.5
	C37	4.26 ± 0.45	3.21 ± 1.47	8.5 ± 0.5	14.1 ± 2.4
1510-089	B6	0.40 ± 0.11	37.45 ± 22.15	24.9 ± 14.8	1.3 ± 1.2
	B8	0.51 ± 0.01	22.38 ± 13.29	11.5 ± 9.9	0.8 ± 1.1
	B9	0.52 ± 0.01	43.21 ± 19.91	28.3 ± 13.4	1.1 ± 0.8

Table 4: Physical Parameters of Jets

Source	D (Gpc)	$\langle\delta\rangle$	$\langle\Gamma\rangle$	$\langle\Theta_o\rangle$ (deg)	$T_{b,int}^{core}$ (10^{10} K)	θ_o (deg)	N
1222+216	2.379	6.6 ± 5.8	24.2 ± 21.0	4.7 ± 1.6	18.15	2.4 ± 1.0	5
3C279	3.080	3.7 ± 6.1	4.9 ± 6	6.6 ± 18.6	74.41	24.8 ± 7.7	5
1510-089	1.919	32.5 ± 8.8	18.5 ± 7.2	1.0 ± 0.2	20.53L	0.3 ± 0.7	3

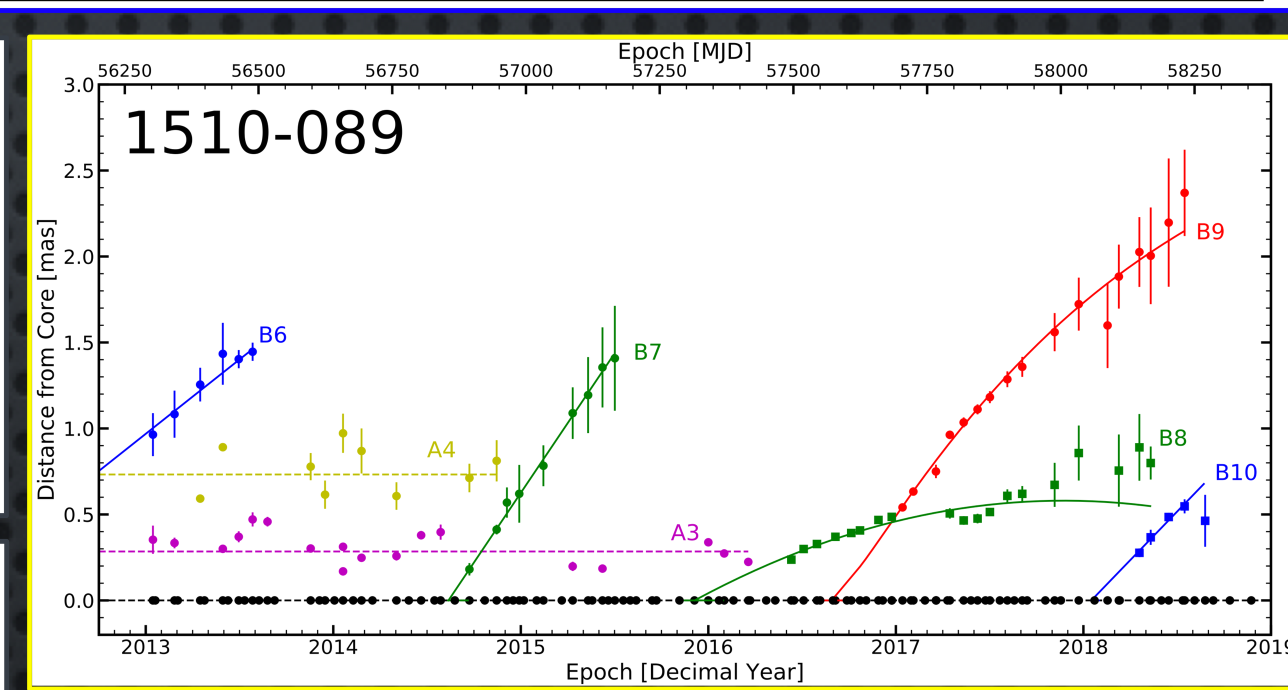

Fig. 7 (above). Separation of jet features from the core of 1510-089 from 2013 Jan. to 2018 Dec. The solid lines or curves represent polynomial fits to the motion, while the dotted line marks the position of the core and quasi-stationary features.. Error-bars show the approximate 1σ positional uncertainties based on $T_{b,obs}$.

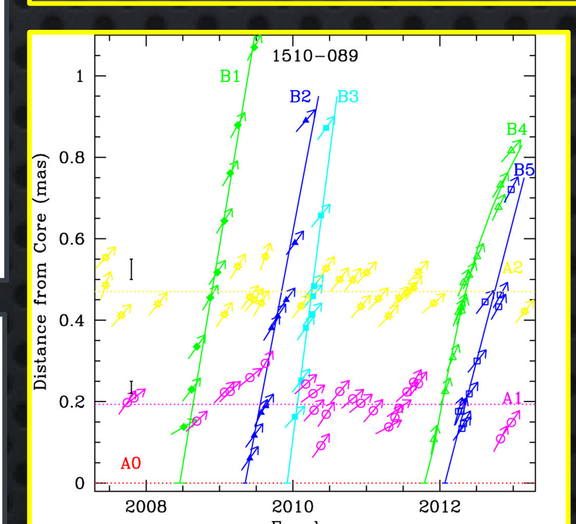

Fig. 8 (left). The separation of jet features from the core of 1510-089 from mid-2007 to mid-2012 (from Jorstad et al. 2017). The vectors show the P.A. of each knot with respect to the core. The vertical black line segments show the approximate 1σ positional uncertainties based on $T_{b,obs}$.

References

Homan, D.C., Ojha, R., Wardle, J.F.C., et al. 2001, ApJ, 549, 840

Jorstad, S.G., Marscher, A.P., Mattox, J.R., et al. 2001, ApJS, 134, 181

Jorstad, S.G., Marscher, A.P., Lister, M.L., et al. 2005, AJ, 130, 1418

Jorstad, S.G., Marscher, A.P., Morozova, D.A., et al. 2017, ApJ, 846, 98

Lister, M.L. 2001, ApJ, 561, 676

Terasranta, H., & Valtaoja, E. 1994, A&A, 283, 51

Fig. 9 (below). Sample sequence of VLBA images of the quasar 1510-089. The size of the restoring beam is 0.19×0.4 mas² at a position angle of -10°. Contours decrease by a factor of $\sqrt{2}$ with respect to the peak flux density across all epochs, 4277 mJy beam⁻¹ on 2016 Jan 01. Straight lines across the images show the positions of the core *A0*.